Available online at www.sciencedirect.com
SCIENCE DIRECT®
International Journal of Heat and Fluid Flow 24 (2003) 807–815
International Journal of HEAT AND FLUID FLOW
www.elsevier.com/locate/ijhff

Local heat transfer around a wall-mounted cube at 45° to flow in a turbulent boundary layer

Hajime Nakamura *, Tamotsu Igarashi, Takayuki Tsutsui

Department of Mechanical Engineering, National Defense Academy, 1-10-20 Hashirimizu, Yokosuka, Kanagawa 239-8686, Japan

Received 9 October 2002; accepted 19 May 2003

Abstract

The flow and local heat transfer around a wall-mounted cube oriented 45° to the flow is investigated experimentally in the range of Reynolds number 4.2×10^3–3.3×10^4 based on the cube height. The distribution of local heat transfer on the cube and its base wall are examined, and it is clarified that the heat transfer distribution under the angled condition differs markedly to that for cube oriented perpendicular to the flow, particularly on the top face of the cube. The surface pressure distribution is also investigated, revealing a well-formed pair of leading-edge vortices extending from the front corner of the top face downstream along both front edges for $Re > (1-2)\times10^4$. Regions of high heat transfer and low pressure are formed along the flow reattachment and separation lines caused by these vortices. In particular, near the front corner of the top face, pressure suction and heat transfer enhancement are pronounced. The average heat transfer on the top face is enhanced at $Re > (1-2)\times10^4$ over that of a cube aligned perpendicular to the flow.

Keywords: Forced convection; Heat transfer; Turbulent boundary layer; Cube; Leading edge vortex

1. Introduction

The flow around a three-dimensional block is dominated by horseshoe vortices with flow separation and reattachment, and as such is extremely complex. Many studies have been performed on the flow structure around a cubical obstacle, as the simple example, e.g., by Castro and Robins (1977) and Ogawa et al. (1983a,b). Most of these studies have been focused on wind loading or the wind environment around large-scale structures such as buildings. The increasing importance on the electronic equipment cooling has given rise to a need for detailed studies on the flow and heat transfer characteristics around small-scale three-dimensional blocks. At present there are remarkably few studies on local heat transfer around a three-dimensional object. Chyu and Natarajan (1991) investigated the distribution of local mass transfer on the surface of a wall-mounted cube using a naphthalene sublimation technique, and later (Natarajan and Chyu, 1994) investigated the effect of orientation with respect to the flow. In these studies, the range of Reynolds number examined, based on the cube height, was 3.1×10^4–1.1×10^5. Meinders et al. (1999) investigated the distribution of local heat transfer on the surface of a cube placed in a developing turbulent channel flow at Reynolds numbers based on the cube height of 2.75×10^3–4.97×10^3. Nakamura et al. (2001) investigated the distribution of the local heat transfer for a wall-mounted cube in a turbulent boundary layer at Reynolds numbers based on the cube height from 4.2×10^3 to 3.3×10^4. The studies of Chyu and Natarajan (1991), Meinders et al. (1999), and Nakamura et al. (2001) showed similar features in the heat/mass transfer distribution on the surface of the cube, although they were performed for different conditions of the boundary layer and different ranges of Reynolds number.

As indicated by Castro and Robins (1977) and Ogawa et al. (1983a,b), there is a remarkable change in the flow pattern on the top face when the cube is angled with respect to the flow direction. However, it appears that the local heat transfer of a cube oriented at an angle

* Corresponding author. Tel.: +81-46-841-3810; fax: +81-46-844-5900.
E-mail address: nhajime@nda.ac.jp (H. Nakamura).

0142-727X/$ - see front matter © 2003 Elsevier Inc. All rights reserved.
doi:10.1016/S0142-727X(03)00087-0

Nomenclature

Cp	pressure coefficient $= (p - p_0)/0.5\rho u_0^2$
d	cube height
h	local heat transfer coefficient $= \dot{q}/(\theta_w - \theta_0)$
$\bar{h}$	face-averaged heat transfer coefficient
Nu	local Nusselt number $= hd/\lambda$
$\overline{Nu}$	face-averaged Nusselt number $= \bar{h}d/\lambda$
Nu_m	overall Nusselt number of a cube
p_0	static pressure at free-stream
p	static pressure on a wall
$\dot{q}$	heat flux
Re	Reynolds number $= u_0 d/v$
u_0	free-stream velocity
x, y, z	streamwise, vertical and cross-stream coordinates

Greeks

α	orientation angle of the cube
δ	boundary layer thickness
θ_0, θ_w	free-stream temperature and wall temperature
λ	thermal conductivity of fluid
v, ρ	kinematic viscosity and density of fluid

Subscripts

f, r, t	front, rear, top faces

to the flow has not yet been investigated, with the analysis of local mass transfer measurement by Natarajan and Chyu (1994) being the most relevant report, showing a greatly change in the mass transfer distribution with the orientation to the flow. In the present study, the flow and local heat transfer around a wall-mounted cube set 45° to the flow in a turbulent boundary layer are investigated. The purpose of the present study is to clarify the Nusselt number distribution on the cube and its base wall, from a direct measurement of heat transfer. A dependency of the Nusselt number with the Reynolds number was investigated in the range of Reynolds number of 4.2×10^3–3.3×10^4, which is lower than that of the previous report by Natarajan and Chyu ($Re = 3.1 \times 10^4$–1.1×10^5).

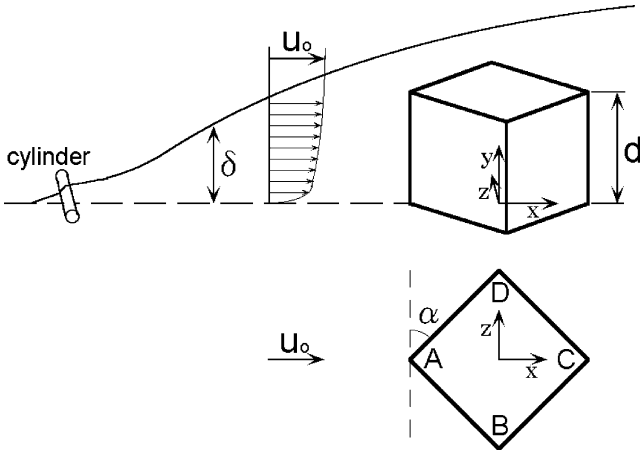

Fig. 1. Coordinate system and symbols.

2. Experimental apparatus and procedure

Fig. 1 shows the coordinate system employed, defined in reference to the wall-mounted cube. Experiments were conducted in a low-speed wind tunnel with a working section of 400 mm high, 300 mm wide and 800 mm long. A cube of height 30 mm (d) was mounted at an angle of $\alpha = 45°$ with respect to the flow on the floor of the wind tunnel. The free-stream velocity u_0 ranged from 2.2 to 17.3 m/s, with a corresponding Reynolds number based on the cube height of 4.2×10^3–3.3×10^4. The turbulent intensity of the free-stream in this range was about 0.5%. The turbulent boundary layer was achieved by attaching a cylinder of 10 mm in diameter to the floor of the chamber 500 mm upstream of the cube. The boundary layer thickness δ was 45–55 mm at the leading edge of the cube, which is thicker than the cube height.

Fig. 2(a) shows the mean velocity distributions in the turbulent boundary layer for different free-stream velocities. The friction velocity u^* was deduced from the following relationship, as shown by Schlichting (1968)

$$u^{*2} = \frac{\tau_0}{\rho} = 0.0225 u_0^{\frac{7}{4}} \left(\frac{v}{\delta}\right)^{\frac{1}{4}}. \tag{1}$$

The solid line in Fig. 2(a) denotes the distribution of experimental universal velocity on a flat plate turbulent boundary layer at zero pressure gradient, also shown by Schlichting (1968)

$$\frac{\bar{u}}{u^*} = 5.85 \log\left(\frac{yu^*}{v}\right) + 5.56. \tag{2}$$

In the range of $yu^*/v > 30$, for which Eq. (2) is valid, the velocity distributions at $u_0 = 2.2$ and 4.1 m/s agree well with Eq. (2), although the velocities at $u_0 = 8.3$ and 16.6 m/s are somewhat higher (within 7%). This scatter may be due to the insufficient distance from the circular cylinder, remaining an effect of the unique velocity distribution of the separated flow from the cylinder. For $5 < yu^*/v < 30$, the intermediate range between turbulent core and laminar sub-layer, the measured velocity decreases and approaches the curve for laminar flow. The scatter within 7% in the turbulent core may not

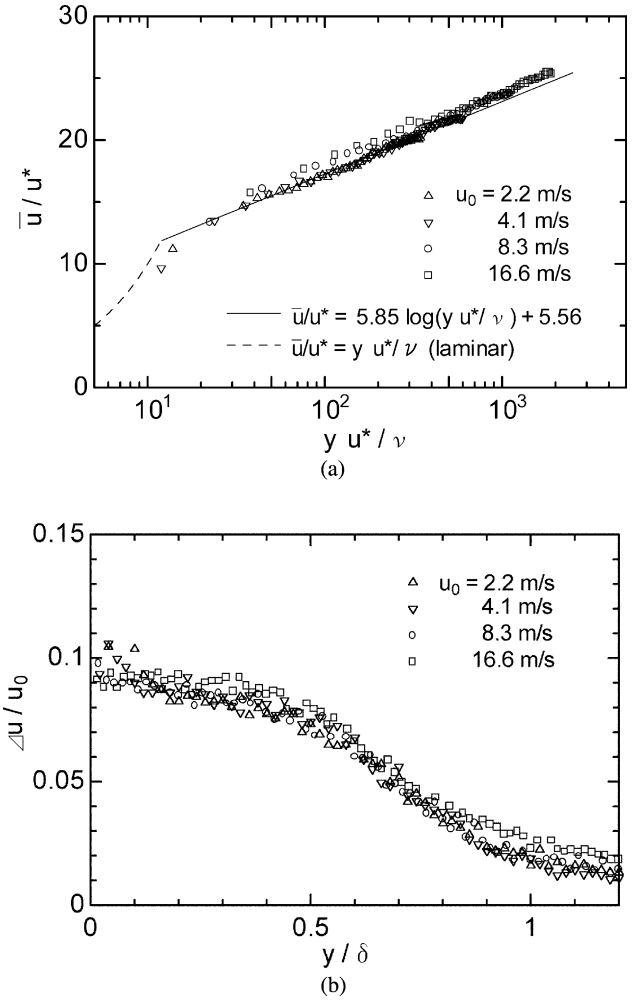

Fig. 2. Velocity distributions in turbulent boundary layer for different free-stream velocities: (a) mean velocity and (b) fluctuating velocity.

affect the heat transfer around the cube significantly, because the turbulent boundary layer diminishes the effect of inflow conditions, as shown by Castro and Robins (1977). Fig. 2(b) shows the distributions of root mean square values of fluctuating velocity in the turbulent boundary layer. The profiles scatter by about 20% but are almost similar regardless of the free-stream velocity.

Visualization of the surface flow on the cube and its base wall was performed using an oil-film method. The pressure distribution on the cube and base wall were measured by multi-tube manometers connected with pressure taps of 0.6 mm in diameter, positioned at 4 mm intervals on the cube faces and 2.5–10 mm intervals on the base wall. In order to obtain the pressure distribution over the entire area, measurements were performed using several test models having pressure taps at different positions. All measuring points from the test models are shown schematically in Fig. 4(a). The uncertainty level of the pressure coefficient *Cp* associated with the measurement method was ±0.01 at $Re = 3.1 \times 10^4$.

Fig. 3(a) and (b) show the test model for the local heat transfer measurement. The cube and base wall were fabricated from acrylic resin plates of 3 and 5 mm thickness, respectively. The faces of the cube and base wall were covered with five stainless steel sheets of 0.02 mm in thickness and 30 mm in width. The middle sheet simultaneously covered three faces of the cube and the base wall. The stainless steel sheets were connected in series electrically and heated by applying an alternating current under the condition of constant heat flux. The temperature difference between the heated surface and the free stream was about 10 °C. Copper–constantan thermocouples of 0.1 mm in diameter were attached to the rear of the stainless steel sheets over one quarter of the sheet area at 3 mm intervals on the cube faces and 4–8 mm intervals on the base wall. In order to obtain the temperature distribution over the entire area, measurements were performed four times under the same experimental conditions by rotating the cube 90° along the vertical axis at the center of the cube. All measuring points from four measurements are shown schematically in Fig. 4(b).

The heat loss by conduction from the heater to the acrylic resin was estimated using thermocouples attached to the interior surfaces of the cube, reverse surface of the base wall, and unheated faces of the cube. The heat loss was calculated by heat conduction analysis. The effect of conduction along the thermocouple leads on temperature measurement was also estimated using the method presented by Satyamurthy et al. (1979). The heat transfer coefficient was calculated taking the above losses into account. If an unheated face

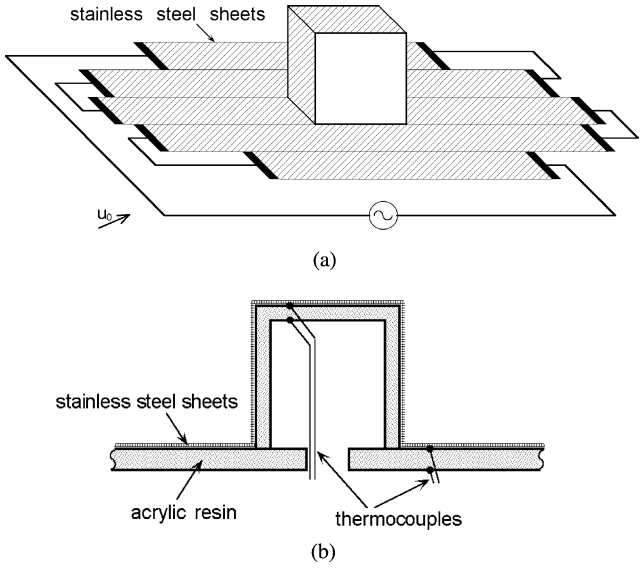

Fig. 3. Experimental model for local heat transfer measurement: (a) exterior view and (b) cross-sectional view.

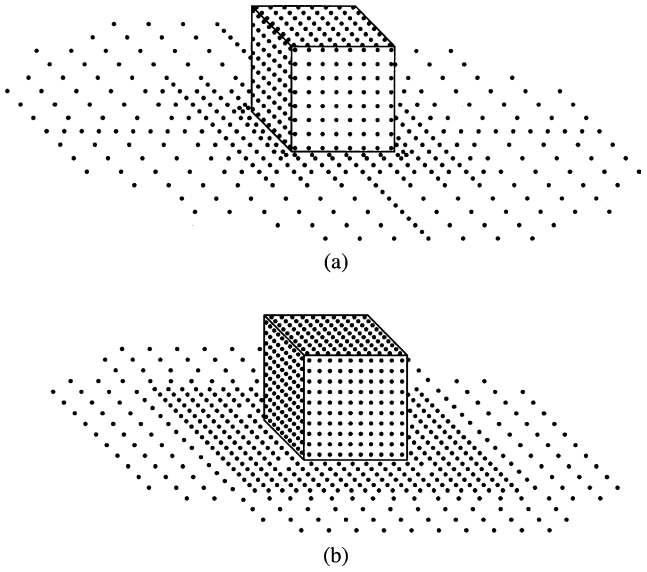

Fig. 4. Schematic views of the sum of measuring points: (a) pressure and (b) temperature.

situates upstream of a measuring point, then heat transfer may increase due to the lower temperature of the inflowing air. However, for the present configuration, this effect is considered to be small, because the surface flow on the unheated face of the cube separates at the downstream edge, and does not directly reach the measuring points.

The experimental uncertainties were calculated using standard uncertainty analysis methods proposed by Kline (1985). The uncertainty of the temperature difference between the wall and free stream ranged from 1% to 2% depending on the wall temperature, and the uncertainty of the input heat flux was within 1%. The uncertainty of heat losses with respect to the local heat transfer coefficient was within 5%, which was estimated from an uncertainty of temperature distribution between the measured points on the unheated faces of the cube, the interior surfaces of the cube, and reverse surface of the base wall. The total uncertainty for the heat transfer coefficient was therefore within 5.5%.

The overall heat transfer for the cube was measured using a constant wall-temperature model, as shown in Fig. 5. A cube of height 30 mm was fabricated from copper and implanted with a heater. The temperature difference between the heated cube surface and the free stream was about 6 °C. Heat loss to the base wall and leads was suppressed by laying a 3 mm thick sheet of balsa wood below the cube. A stainless steel sheet was set under the balsa sheet as a sub-heater, which was heated to the same temperature as the cube. The uncertainty of the overall heat transfer coefficient was within 1.1%.

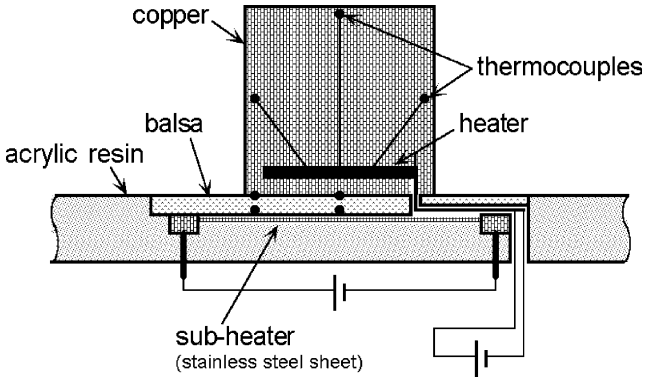

Fig. 5. Experimental model for overall heat transfer measurement.

3. Fluid flow around a cube

3.1. Surface oil-film pattern

A typical surface oil-film pattern around the cube is shown in Fig. 6(a) and (b), and sketches of the surface

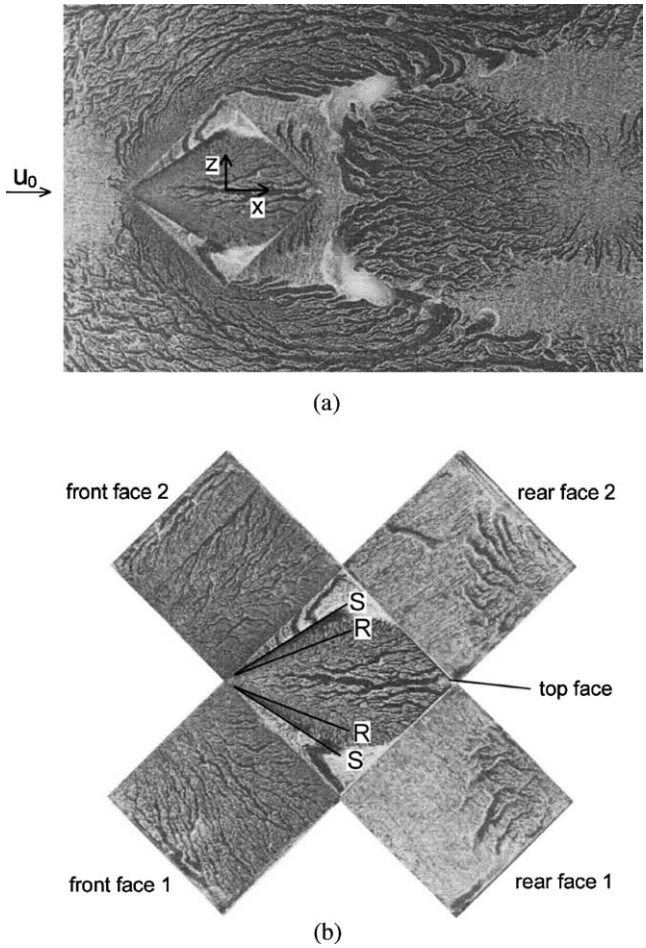

Fig. 6. Surface oil-film pattern around the cube at $Re = 3.1 \times 10^4$: (a) top view and (b) cube.

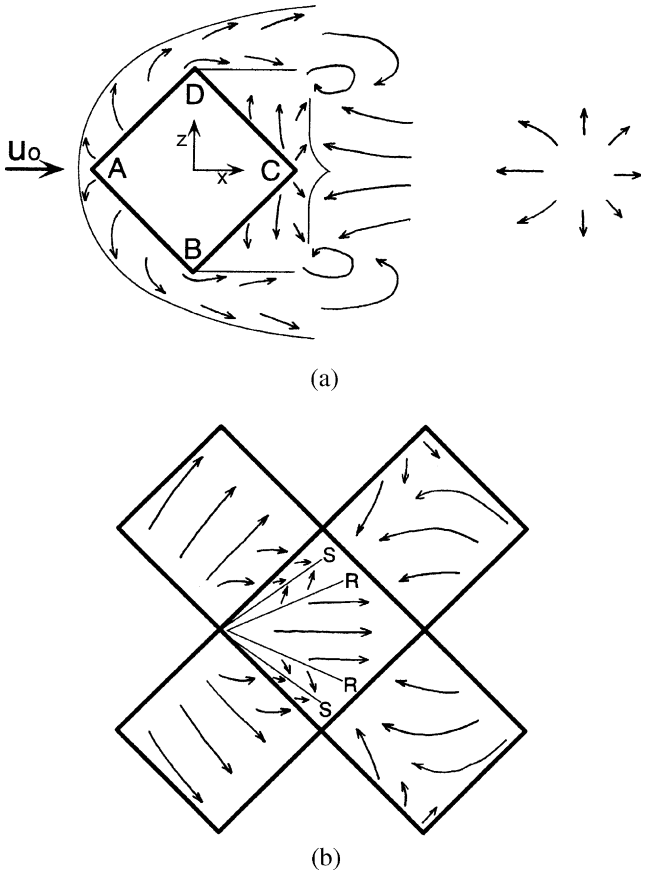

Fig. 7. Sketch of surface flow pattern at $Re = 3.1 \times 10^4$: (a) base wall and (b) cube.

flow obtained by the oil-film pattern and smoke visualization are shown in Fig. 7(a) and (b). On the base wall, a horseshoe pattern that extends from the front of the cube out to both sides is formed. On the top face of the cube, a pair of flow separation lines (S) can be clearly seen extending from the front corner downstream along both edges. A pair of flow reattachment lines (R) exists inside the separation lines. The feature on the top face indicates the formation of a pair of leading-edge vortices, characteristic of the flow pattern of a delta wing at high angle of attack, as shown in Fig. 8 (Nakaguchi, 1984). A similar top-face flow structure was reported by Castro and Robins (1977), Ogawa et al. (1983b), and Natarajan and Chyu (1994), for higher Reynolds numbers ($>3\times10^4$). A wedge flow forms on the front faces of the cube and separates at the edges on both sides. In the upper part of each of the front faces, an upward flow representing the origin of the leading edge vortex on the top face can be seen. On the base wall behind the cube, the separated flow reattaches at around $x/d = 2.7, z = 0$, which is very close to the result obtained by Ogawa et al. (1983a) for higher Reynolds numbers ($>10^5$). A recirculating flow is formed between the flow reattachment region and the cube, inducing an upward flow on the

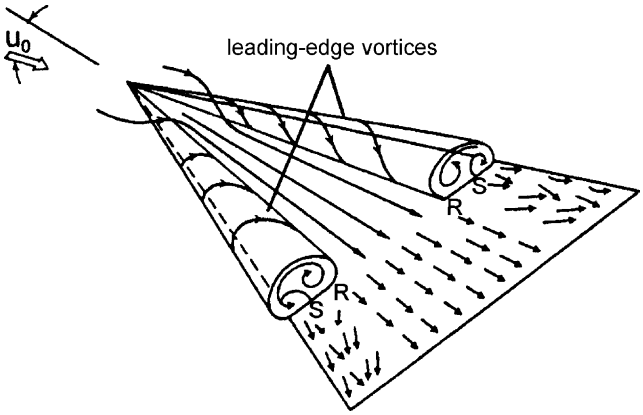

Fig. 8. Flow on delta wing at high angle of attack.

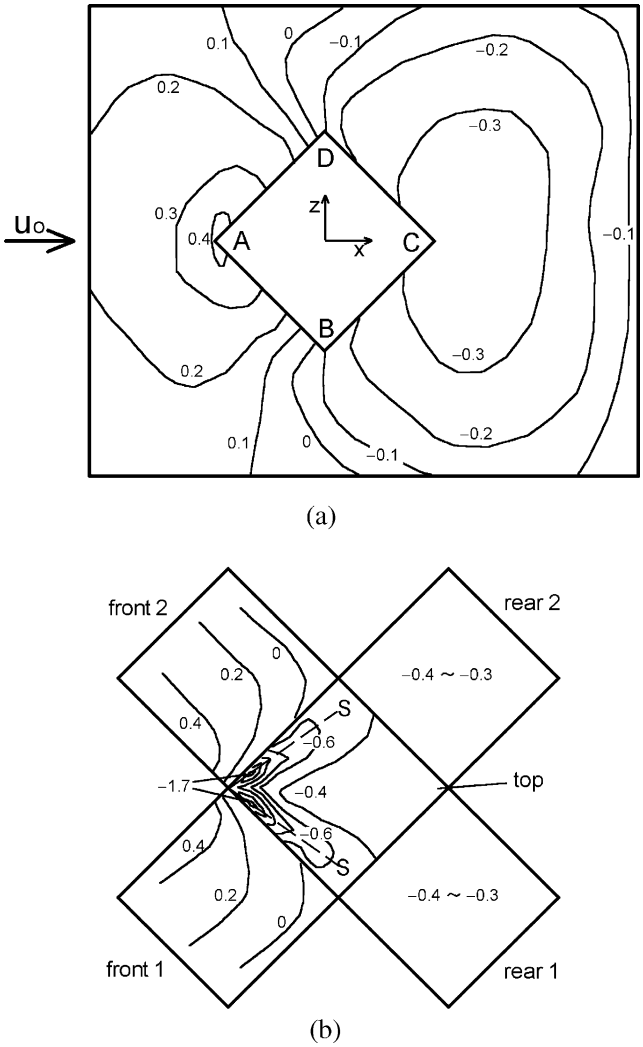

Fig. 9. Contours of pressure coefficient at $Re = 3.1 \times 10^4$: (a) base wall and (b) cube.

rear face of the cube. Interaction between the horseshoe vortex and the separated flow produces an arch vortex

behind the cube, resulting in the formation of a pair of oil contaminating points at $x/d = 1.0$, $z/d = \pm 0.7$.

3.2. Pressure distribution

Fig. 9(a) and (b) show the contours of the mean pressure coefficient on the base wall and the cube. On the base wall and the front faces of the cube, the regions of maximum pressure are formed around the front corner of the cube, and the pressure coefficient decreases in the flow direction. On the base wall behind the cube and on the rear faces of the cube, representing the separated flow region, Cp is negative. On the top face of the cube, a pair of extremely low pressure points of $Cp = -1.7$ exist near the front corner. These points occur due to the leading edge vortices, and the regions of low pressure extend downstream along the flow separation lines of the leading edge vortices. Kawai (2002) reported that the surface pressure near the front corner of the top face of a square block at $\alpha = 45°$ fluctuates violently and the magnitude of the suction peak occasionally reaches $Cp = -4$ to -5.

4. Heat transfer

4.1. Distribution of local heat transfer

Contours of the local Nusselt number around the cube at $Re = 3.3 \times 10^4$ are shown in Fig. 10(a) and (b). The reference length for the Nusselt number is defined by the cube height d. On the top face of the cube, the Nusselt number is extremely high near the front corner. The maximum Nusselt number in this region is about 350, which is more than three times that at the base wall far from the cube. A pair of higher Nusselt number regions extends downstream along the flow reattachment lines of the leading edge vortices. This Nusselt number distribution on the top face is similar to the mass transfer distribution obtained by Natarajan and Chyu (1994) for a higher Reynolds number of 8.2×10^4. With increasing Reynolds number, the flow reattachment lines tend to shift toward the edges. The feature on the top face differs markedly to that for the cube perpendicular to the flow, shown in Fig. 11(b), investigated in the previous study by Nakamura et al. (2001). On the front and rear faces of the cube, the Nusselt number decreases in the direction of surface flow due to the development of a thermal boundary layer. The Nusselt number on the base wall in the horseshoe vortex region is approximately twice as high as that far from the cube, but lower than that ($Nu = 300$) for $\alpha = 0°$, shown in Fig. 11(a), obtained by Nakamura et al. (2001) under the same flow conditions. On the base wall behind the cube, the heat transfer is enhanced in the flow reattachment region ($x/d > 1.5$), while a pair of minimum Nusselt

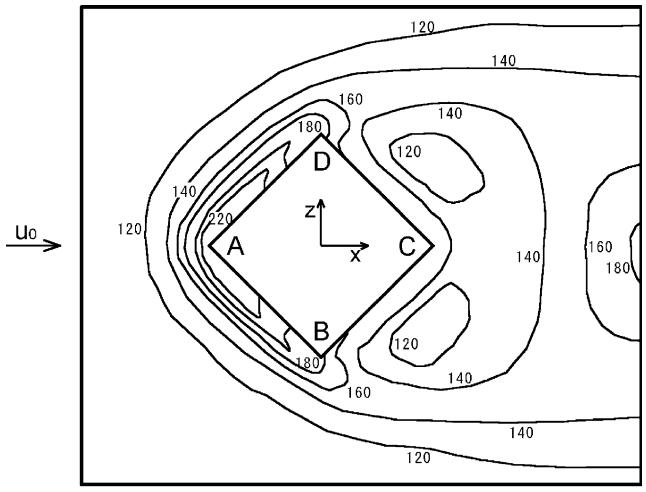

(a)

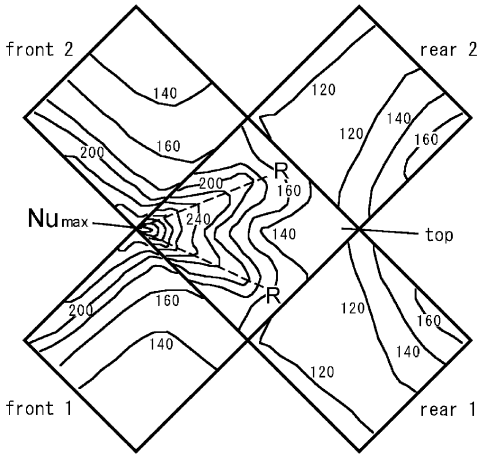

(b)

Fig. 10. Contours of local Nusselt number at $Re = 3.3 \times 10^4$: (a) base wall and (b) cube.

number regions due to the arch vortex is formed at $x/d = 0.6$, $z/d = \pm 0.6$. These base wall features are similar to the mass transfer distribution obtained by Chyu and Natarajan (1996) at $Re = 1.7 \times 10^4$.

Fig. 12(a) and (b) show the Nusselt number distributions at $Re = 8.3 \times 10^3$. The features are very similar to those for $Re = 3.3 \times 10^4$, except on the top face of the cube. For $Re = 8.3 \times 10^3$, the maximum Nusselt number occurs at the front edge of the front faces, not on the top face, and the pair of high Nusselt number regions on the top face is not clear. This indicates that the leading edge vortices are not clearly formed at lower Reynolds numbers. In the present study, the pair of high Nusselt number regions associated with the leading edge vortices clearly formed at Reynolds numbers of greater than $(1–2) \times 10^4$.

The Nusselt number distributions on the front and rear faces for given heights, y/d, at $Re = 3.3 \times 10^4$ are presented in Fig. 13. The profiles of each face have

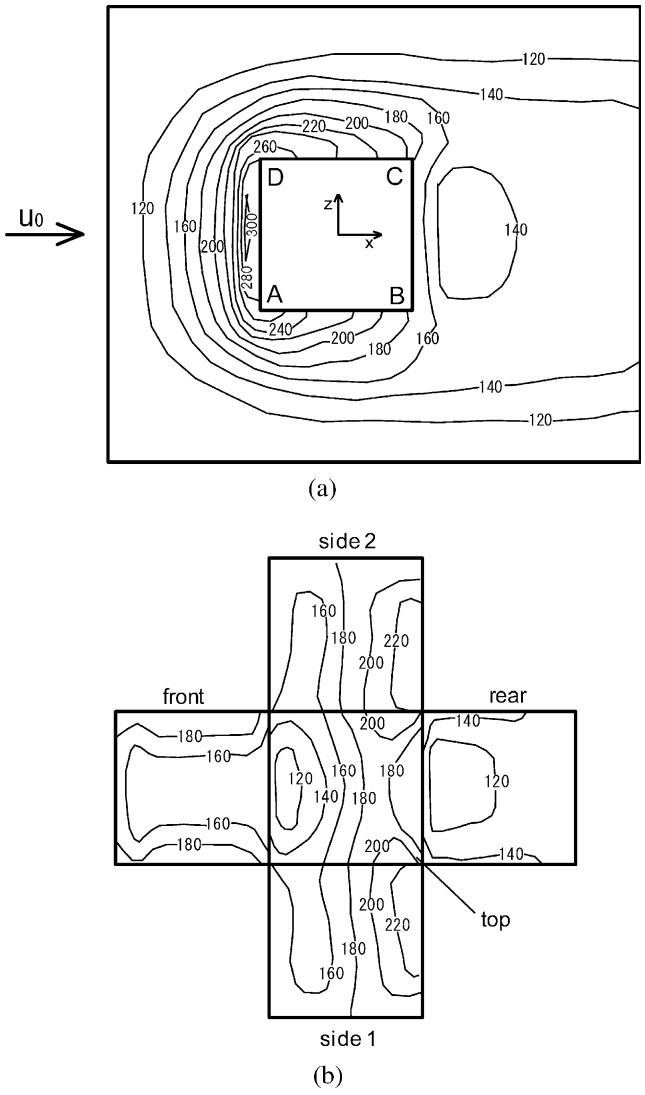

Fig. 11. Contours of local Nusselt number at $Re = 3.3 \times 10^4$ for $\alpha = 0°$ from Nakamura et al. (2001): (a) base wall and (b) cube.

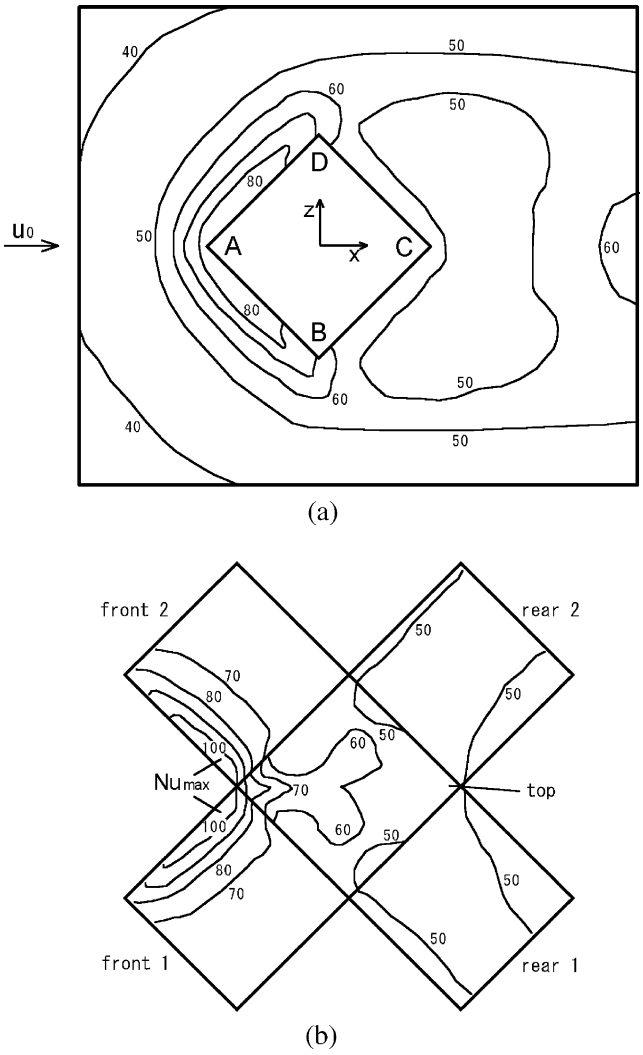

Fig. 12. Contours of local Nusselt number at $Re = 8.3 \times 10^3$: (a) base wall and (b) cube.

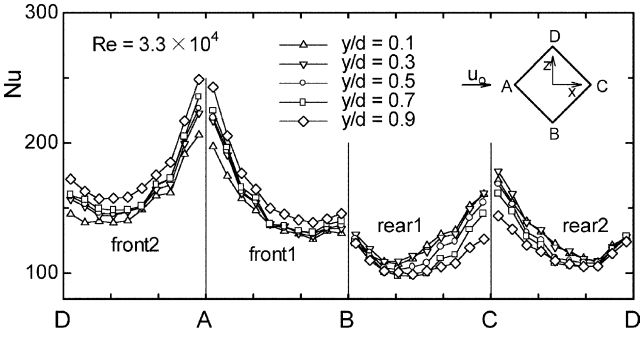

Fig. 13. Distribution of local Nusselt number on front and rear faces of the cube for various heights y/d at $Re = 3.3 \times 10^4$.

distinctive features, and change very little with height. This indicates that the distribution of local heat transfer is close to two-dimensional. On the front faces, the Nusselt number decreases in the direction of surface flow from the front corner A to the side corners B and D. The Nusselt number increases slightly near the side edges B and D, probably due to the thinning of the thermal boundary layer caused by the separation of the surface flow at edges B and D. The Nusselt number in the upper part of $y/d = 0.9$ on the front faces is higher due to the acceleration of the flow toward the low pressure region formed by the leading edge vortices. Fig. 14 shows the variation in the Nusselt number distributions with Reynolds number at the middle height of $y/d = 0.5$. It can be seen that the characteristics of the heat transfer distribution on both the front and rear faces do not change with the Reynolds number. Fig. 15 shows a comparison of the Nusselt number distribution at $y/d = 0.5$ with that for an effectively two-dimensional square prism in a free stream obtained by Igarashi (1985, 1986). On the front faces, the value of the Nusselt number for the cube is higher than that for the square prism. This difference is considered to depend mainly on

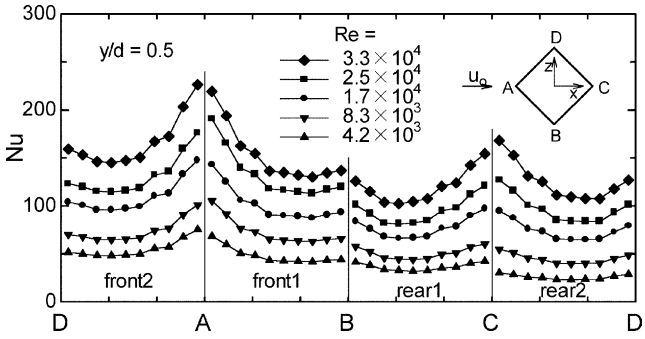

Fig. 14. Distribution of local Nusselt number on front and rear faces of the cube at $y/d = 0.5$ for $Re = 4.2 \times 10^3$–3.3×10^4.

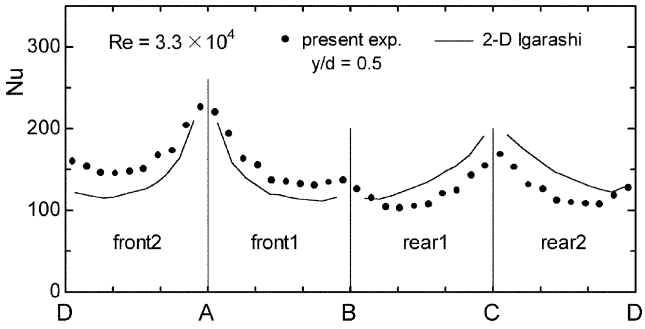

Fig. 15. Comparison of local Nusselt number distribution of present configuration with that for an effectively two-dimensional square prism in a free stream.

heat transfer enhancement by the horseshoe vortex. In contrast, the Nusselt number on the rear face of the square prism is higher, attributed to the greater enhancement of heat transfer by two-dimensional vortex shedding compared to three-dimensional vortex shedding for the cube.

4.2. Average heat transfer

Fig. 16 shows the face-averaged Nusselt number on the front and rear faces (average of both faces) and top face of the cube. The Nusselt number on each face is then expressed as

Front face: $\overline{Nu_f} = 0.52Re^{0.55}$

Rear face: $\overline{Nu_r} = 0.11Re^{0.67}$

Top face: $\overline{Nu_t} = 0.029Re^{0.84}$

When $Re < 2 \times 10^4$, the average Nusselt number is highest on the front face, followed by the top and rear faces. On the front and rear faces, the average Nusselt numbers are almost equal (within 5%) to those for $\alpha = 0°$. The exponent of the Reynolds number on the front face is slightly higher than 0.5 for a face in a laminar flow, probably due to the effect of inflow turbulence and the horseshoe vortex. The exponent on the rear face is 0.67, which is equivalent to the 2/3 of separated flow behind bluff bodies, as shown by Richardson (1963) and Igarashi et al. (1975). On the top face, the exponent is much higher than for the other faces, which is related to the fact that the appearance of the leading edge vortices depends strongly on the Reynolds number, as shown in Figs. 10 and 12. It is suggested that the intensity of rotation of the leading edge vortex increases with the Reynolds number, leading to intense flow reattachment and resulting in a remarkable increase in heat transfer on the top face. The Nusselt number on the top face is higher than that for $\alpha = 0°$ at $Re > (1–2) \times 10^4$, at which the leading edge vortices are clearly formed.

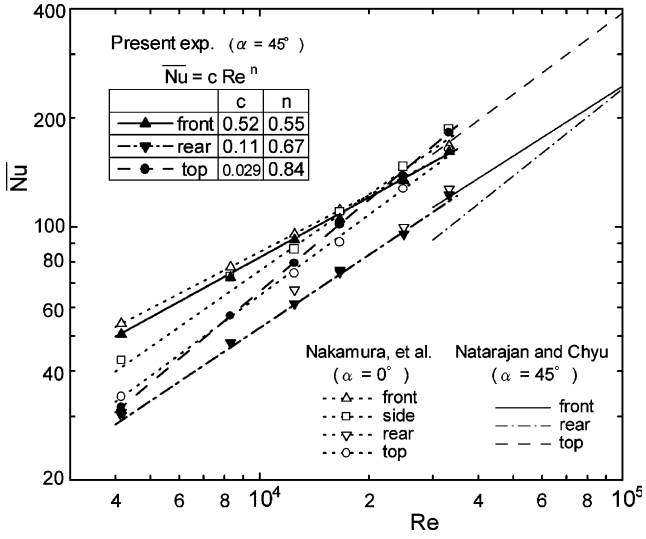

Fig. 16. Average Nusselt number on individual faces of a wall-mounted cube.

The overall Nusselt number of the cube is shown in Fig. 17 compared to that for $\alpha = 0°$. The Nusselt number obtained using the constant temperature model is also shown. The Nusselt numbers for the constant heat-flux model and the constant wall-temperature model are in good agreement (±2%) for both $\alpha = 0°$ and 45°, indicating that the effect of the thermal boundary condi-

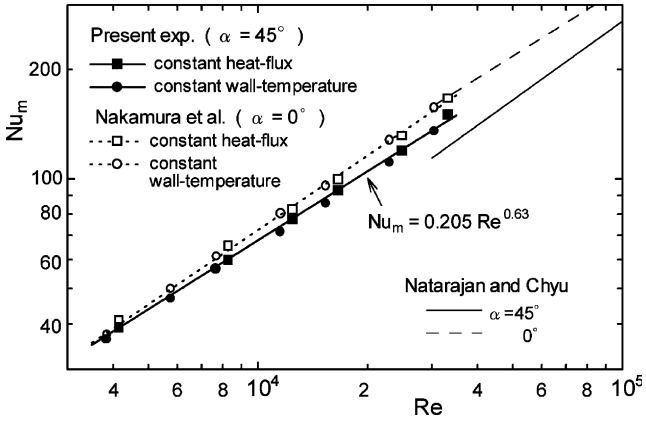

Fig. 17. Overall Nusselt number of a wall-mounted cube.

tion is small. For $\alpha = 45°$, the overall Nusselt number for the cube is expressed as

$$\text{Overall}: \quad Nu_m = 0.205Re^{0.63} \ (Re = 4.2 \times 10^3\text{–}3.3 \times 10^4)$$

The overall Nusselt number for $\alpha = 45°$ is therefore about 10% lower than that for $\alpha = 0°$ in the present range of Reynolds numbers.

These results are compared with those obtained by Natarajan and Chyu (1994) in Figs. 16 and 17. The Sherwood number obtained by Natarajan and Chyu was converted into a Nusselt number by using an analogy between heat and mass transfer according to the relationship presented by Natarajan and Chyu (1994). At $Re = 3.3 \times 10^4$, the overall Nusselt number for $\alpha = 45°$ obtained by Natarajan and Chyu is 15% lower than that for the present study, although the results for $\alpha = 0°$ are consistent. The reason for the difference for $\alpha = 45°$ is not clear. However, the exponent of the Reynolds number obtained by Natarajan and Chyu for $\alpha = 45°$ is 0.719, which is thought to be too high compared to the 0.626 obtained for $\alpha = 0°$. If the correlation obtained in the present study is extended to $Re = 1.1 \times 10^5$, the highest Reynolds number examined by Natarajan and Chyu, the overall Nusselt numbers for $\alpha = 45°$ are almost coincident. This suggests that the present correlations are valid.

5. Conclusions

An experimental study was performed on the flow and local heat transfer around a wall-mounted cube oriented 45° to flow at Reynolds numbers of 4.2×10^3–3.3×10^4. The thickness of the turbulent boundary layer was thicker than the height of the cube. The main results are as follows.

(1) The heat transfer distribution differs markedly from that for a cube aligned perpendicular to the flow, particularly on the top face. In this case, a pair of leading edge vortices were formed, extending from the front corner of the top face downstream along both front edges. These leading edge vortices only appear at Reynolds numbers greater than $(1-2) \times 10^4$.
(2) Regions of high heat transfer and low pressure are formed along the flow reattachment and separation lines of these leading edge vortices, and the pressure suction and heat transfer enhancement are pronounced near the front corner of the top face.
(3) The average Nusselt number on each face of the cube was found to be expressed as

$$\text{Front face:} \quad \overline{Nu_f} = 0.52Re^{0.55}$$

$$\text{Rear face:} \quad \overline{Nu_r} = 0.11Re^{0.67}$$

$$\text{Top face:} \quad \overline{Nu_t} = 0.029Re^{0.84}$$

The exponent of the Reynolds number on the top face is higher than for the other faces, attributed to the increased intensity of rotation of the leading edge vortices with increasing Reynolds number.
(4) The overall Nusselt number of the cube was expressed as follows.

$$\text{Overall}: \quad Nu_m = 0.205Re^{0.63} \ (Re = 4.2 \times 10^3\text{–}3.3 \times 10^4)$$

This value is about 10% lower than that for a cube oriented perpendicular to the flow in the present range of Reynolds numbers.

References

Castro, I.P., Robins, A.G., 1977. The flow around a surface-mounted cube in uniform and turbulent streams. J. Fluid Mech. 79 (2), 307–335.

Chyu, M.K., Natarajan, V., 1991. Local heat/mass transfer distributions on the surface of a wall-mounted cube. Trans. ASME J. Heat Transfer 113, 851–857.

Chyu, M.K., Natarajan, V., 1996. Heat transfer on the base surface of three-dimensional protruding elements. Int. J. Heat Mass Transfer 39 (14), 2925–2935.

Igarashi, T., Hirata, M., Nishiwaki, N., 1975. Heat transfer in separated flows, Part 1 experiments on local heat transfer from the rear of a flat plate inclined to an air stream. Heat Transfer Japanese Res. 4 (1), 11–32.

Igarashi, T., 1985. Heat transfer from a square prism to an air stream. Int. J. Heat Mass Transfer 28 (1), 175–181.

Igarashi, T., 1986. Local heat transfer from a square prism to an airstream. Int. J. Heat Mass Transfer 29 (5), 777–784.

Kawai, H., 2002. Local peak pressure and conical vortex on building. J. Wind Eng. Ind. Aerodyn. 90, 251–263.

Kline, S.J., 1985. The purposes of uncertainty analysis. Trans. ASME J. Fluid Eng. 107, 153–160.

Meinders, E.R., Hanjalic, K., Martinuzzi, R.J., 1999. Experimental study of the local convection heat transfer from a wall-mounted cube in turbulent channel flow. Trans. ASME J. Heat Transfer 121, 564–573.

Nakaguchi, H., 1984. Nagare. Jpn. Soc. Mech. Eng., Maruzen. p. 85 (in Japanese).

Nakamura, H., Igarashi, T., Tsutsui, T., 2001. Local heat transfer around a wall-mounted cube in the turbulent boundary layer. Int. J. Heat Mass Transfer 44, 3385–3395.

Natarajan, V., Chyu, M.K., 1994. Effect of flow angle-of-attack on the local heat/mass transfer from a wall-mounted cube. Trans. ASME J. Heat Transfer 116, 552–560.

Ogawa, Y., Oikawa, S., Uehara, K., 1983a. Field and wind tunnel study of the flow and diffusion around a model cube—I. Flow measurements. Atmos. Environ. 17 (6), 1145–1159.

Ogawa, Y., Oikawa, S., Uehara, K., 1983b. Field and wind tunnel study of the flow and diffusion around a model cube—II. Nearfield and cube surface flow and concentration patterns. Atmos. Environ. 17 (6), 1161–1171.

Richardson, P.D., 1963. Heat and mass transfer in turbulent separated flow. Chem. Eng. Sci. 18, 149–155.

Satyamurthy, P., Marwah, R.K., Venkatramani, N., Rohatgi, V.K., 1979. Estimation of error in steady-state temperature measurement due to conduction along the thermocouple leads. Int. J. Heat Mass Transfer 22, 1151–1154.

Schlichting, H., 1968. Boundary Layer Theory, Sixth ed. McGraw-Hill, New York. pp. 598–602.